Multiple nonlinear regression model for predicting the optical performances of dielectric Crossed Compound Parabolic Concentrator (dCCPC)

Meng TIAN[1], Yuehong SU[1,*]

[1] Department of Architecture and Built Environment, Faculty of Engineering, University of Nottingham, University Park, Nottingham NG7 2RD, UK

* Corresponding author: yuehong.su@nottingham.ac.uk

Abstract

As a typical type of three-dimensional compound parabolic concentrator (CPC), dielectric crossed compound parabolic concentrator (dCCPC) has drawn a significant research attention in these years to explore its angular characteristics in solar collection for concentrating photovoltaics and daylighting control in buildings. Optical efficiency and transmittance are the main performance indicators to evaluate a dCCPC which may be base-coated as a receiver or non-coated for daylighting. The most common way to accurately determine the performance of a dCCPC is through ray-tracing simulation which requires advanced optical analysis software and lots of time. To facilitate the annual performance evaluation of dCCPC, this study puts forward several mathematical models for multiple nonlinear regression based on a mass of simulation results. The models can predict the transmittance of non-coated dCCPC and the both of transmittance and optical efficiency of base-coated dCCPC from several sky parameters, respectively. The agreement between predicted and simulated values is generally satisfactory. The coefficient of determination (R^2) for each model is higher than 0.94 and the mean square error (MSE) is less than 0.002. Six specific time among the whole year are selected to verify the reliability of the prediction models in practice. The limitation and significance of these models are discussed as well. The regression models provide a convenient and accurate approach to predict the optical performance of dCCPC.

Highlights

- Mathematical models are proposed to predict the optical performance of dCCPC.
- The process of deducing the models by multiple nonlinear regression are introduced.
- The R^2 of prediction models are higher than 0.94 and MSE are less than 0.2%.
- The models provide a reliable and convenient way for dCCPC performance prediction.

Keywords

Dielectric crossed compound parabolic concentrator (dCCPC), transmittance, optical efficiency, mathematical model, multiple nonlinear regression, clear sky

39

1. Introduction

The compound parabolic concentrator (CPC) is one type of the nonimaging optics, which has great potential in solar energy concentration, daylighting control and illumination. CPC is a non-tracking concentrator to collect solar energy in concentrating photovoltaic (CPV) and solar thermal systems, which has been verified by many research studies (Sellami and Mallick, 2013, Li et al., 2015, Arnaoutakis et al., 2015, Karathanassis et al., 2017). In terms of traditional two-dimensional (2D) CPC, Sun and Shi (Sun and Shi, 2010) tested the maximum short circuit current of a CPV system which was higher than twice of the flat PV panel. In the experiment conducted by Bahaidarah et al. (Bahaidarah et al., 2014), the CPV system with cooling generated 61.9% higher electricity compared to the flat PV panel with cooling. For the lens-walled CPC proposed by Su et al. (Su et al., 2012a) and Li et al.(Li et al., 2013, Li et al., 2014a, Li et al., 2014b), it was found that the solar energy collected by the lens-walled CPC is 20%-30% more than traditional 2D CPC. For crossed CPC (CCPC), the maximum optical efficiency could reach 95% (Sellami et al., 2012). The maximum power ratio was up to 2.67 for the dielectric filled crossed CPC (Baig et al., 2014b). In a system integrating CPC, PV and tubular absorber, the total energy conversion efficiency was 20% higher than the independent PV module (Ulavi et al., 2013).

The advantages of CPC in daylighting control has been also proposed by some researchers (Walze et al., 2005, Yu et al., 2014, Zacharopoulos et al., 2000, Mallick and Eames, 2007, Sarmah and Mallick, 2015) in recent years. Due to its specific structure, CPC can receive or reject sunlight depending on the incident angle. Ulavi et al. (Ulavi et al., 2014b, Ulavi et al., 2014a) designed a hybrid solar window with CPC and tubular absorber; the annual thermal efficiency ranged from 21% to 26% when it was used as skylight and 15% to 24% when it was used as south or east-facing windows. Yu et al. (Yu et al., 2014) investigated the feasibility of using 2D dielectric CPC as skylight in daylighting control. It was found that the CPC provided lower transmittance at noon and higher transmittance in the morning and afternoon under clear sky, which could reduce solar heat gain significantly. PRDIEs is a smart window applied on building facade integrating CPC and photovoltaic to provide daylighting and electricity at the same time. It has been extensively investigated by many researchers (Sarmah and Mallick, 2015, Sarmah et al., 2014, Baig et al., 2014a, Mallick et al., 2004, Mallick et al., 2006) . The average electrical conversion efficiency was 9.43% and it could reduce up to 20% in the cost of per unit power output comparing with the conventional PV module (Sarmah et al., 2014).

Two-dimensional (2D) trough CPC has a longitudinal axis and two parabolic-curved surfaces, which is the most common one in all CPCs (Welford and Winston, 1978). For the most common east-west orientation of 2D trough CPC in practice, the incident light projected on the north-south meridian forms a so-called south projection angle, which could be compared with the acceptance angle of CPC to determine its optical performance. However, this would be not suitable for a three-dimensional CPC, for example, typical crossed CPC (CCPC), also called orthogonal CPC, consists of four parabolic surfaces and two square apertures. Different from 2D CPC, the optical performance of CCPC is more complicated so that it cannot be determined using a simple south projection angle directly. Due to the complex ray path of incident light, the optical performance of CCPC can be obtained only by raytracing simulation.

The dielectric CPC (dCPC) is an alternative to the mirror CPC and has an enlarged acceptance angle owing to the refraction on air-dielectric interface and also allows transmission of light beyond its acceptance angle. As a result, the dCPC has been widely used in CPV and daylighting control systems. Welford and Winston (Welford and Winston, 1978) proposed that the actual acceptance angle of a dCPC needs to be adjusted by a certain degree for nonmeridional incident rays due to the refraction. For 2D dCPC, Yu and Su (Yu and Su, 2015) proposed a concept of inner projection angle which is the refracted projection angle of incident light inside dCPC. They found strong correlations between inner projection angles and optical performance at different solar azimuth angles of 2D dCPC based on simulation results. However, for 3D dielectric crossed compound parabolic concentrator (dCCPC), the refraction and total internal reflection owing to dielectric material should also be considered, which causes the prediction of optical performance of dCCPC becomes more complicated.

To date, no research has been published in the literature that proposes a relatively fast and simple model to predict the optical performance of dCCPC except for simulation. In this study, several mathematical models are proposed through multiple nonlinear regression based on a mass of simulation results, in order to predict the optical performance for base-coated and non-coated dCCPC from the given solar azimuth angle, altitude angle and sky clearness factor. The validation and limitations of the models are given to discuss the feasibility and reliability of the models as well. On basis of the regression models proposed in this study, the transmittance of using dCCPC can be calculated in a fast and accurate way rather than using long time ray-tracing simulations. Similarly, in terms of the CPV application, the amount of light received by the PV panel attached on the base of dCCPC can also be determined in a much more convenient way.

2. Methodology

2.1 CPC Models

The optical performance of dCCPC can be evaluated in two aspects: the optical efficiency and transmittance. According to previous studies (TIAN and SU, 2015, TIAN and SU, 2016), it was found that the transmittance and optical efficiency of a dCCPC are related to its dimension, sun position and sky condition. In this research, the dCCPC demonstrated in Fig. 1 is selected as an example to investigate the correlations between its performance and influencing factors. It consists of four parabolic surfaces and two square apertures, which is transformed by crossed interception of two tough dielectric CPCs. For the purpose of applying CPC to windows or facades, the dCCPC is a miniature optical structure, for example, with a height of 24.2mm and an entry aperture of 18mm*18mm. The dCCPC may be filled with acrylic material, which has a refractive index of 1.5. The inner and outer half acceptance angles of the dCCPC are 14.47° and 22.02°, respectively. Two kinds of the dCCPC in this dimension will be investigated in this study: one is non-coated dCCPC which is the normal dielectric CCPC, the other is base-coated dCCPC having black material attached on its exit aperture to simulate solar absorption.

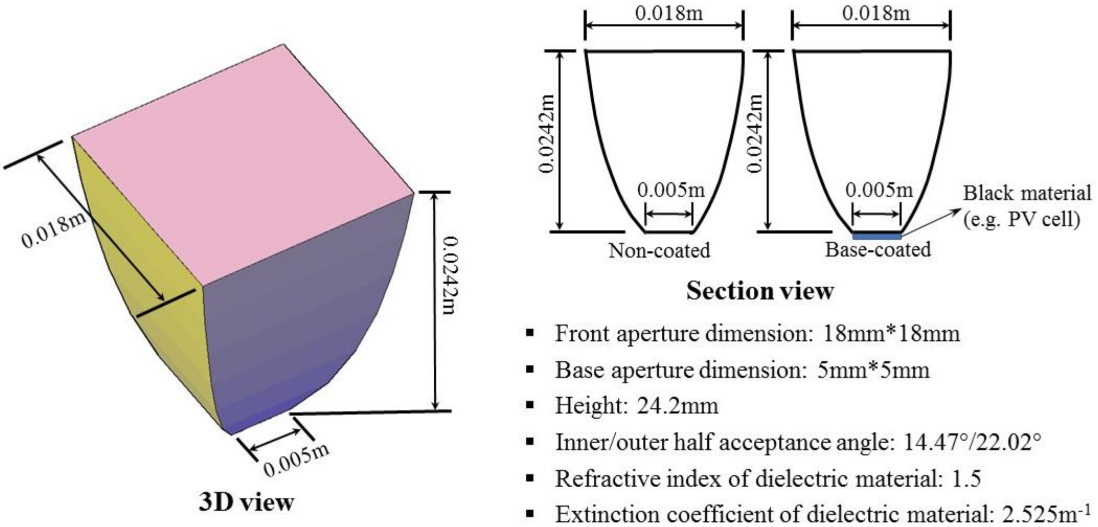

Figure 1. Schematics, dimensions and physical properties of dielectric CCPC

2.2 Software settings

The optical performance of dCCPC was simulated by Photopia. It is a fast and accurate photometric analysis software which can provide liable and comprehensive evaluation for non-imaging optical systems. The calculation is based on probabilistic raytracing under numerous defined optics and light source models in its library (Photopia, n.d.). The light source models for modelling daylight input offered by Photopia are based on the IESNA RP-21 daylight equations. The luminance distribution of sky dome varies across the hemisphere as described in IESNA RP-21. The absolute illuminance from the sun (solar disk) and sky are provided automatically depending on the altitude angles and sky conditions, but they can also be adjusted manually. Both of the sun and sky model emit light onto the optical systems in order to simulate real outdoor conditions. It is worth to mention that the real sky changes all the times and the RP-21 equations represent standard conditions.

Sky clearness factor (ε) proposed by Perez et al. (Perez et al., 1990) is a popular way to determine the sky condition which has been used in EnergyPlus simulation (EnergyPlus, 2016) and daylight calculations (Kleindienst et al., 2008, Piderit et al., 2014). It is calculated from the horizontal diffuse irradiance, normal direct irradiance and solar zenith angle in order to describe the sky condition as shown in Eq. 1. Eight categories corresponding to the different value intervals were proposed to describe the sky conditions from overcast to very clear sky (Perez et al., 1990).

$$\varepsilon = \frac{\frac{(I_h + I)}{I_h} + kZ^3}{1 + kZ^3} \qquad (Eq. 1)$$

where I is direct normal solar irradiance; I_h is diffuse horizontal irradiance; k is a constant and equals 1.041; Z is solar zenith angle in radians.

However, in the optical simulation using Photopia, it is not a setting option to choose a sky clearness factor, but it allows to change the lumen or radiative outputs from the sun disk and sky dome in its sky model. The horizontal irradiance or illuminance can be then obtained from the sun and sky with complex light distribution for different solar altitudes, and the sky clearness factor can be hence calculated. It would offer a convenience in data analysis by defining a term called sunlight lumen ratio (φ_{lumen}), which is a ratio of the direct normal output from the sun disk to the diffuse output from the sky dome in the sky model, as expressed in Eq. 2. The output from the sun and sky can be set as required in Photopia. The values of sunlight lumen ratio can be controlled as constant in order to investigate the relationships among other criteria.

$$\varphi_{lumen} = \emptyset_{sun} : \emptyset_{sky} \quad (Eq. 2)$$

where $\emptyset_{sun}$ is the total light output from the sun (direct light output); $\emptyset_{sky}$ is the total light output from the sky (diffuse light output).

In addition, it is important to note that each sunlight lumen ratio corresponds to an interval of sky clearness factor. Table 1 illustrates the sunlight lumen ratios used in simulation for this study, and corresponding horizontal sunlight illuminance ratio, sky clearness factors and sky conditions. The horizontal sunlight illuminance ratio is the ratio of direct horizontal illuminance and global horizontal illuminance, which can indicate the percentage of sunlight illuminance to the total illuminance on a horizontal surface. According to the classification of clearness factor, it is overcast condition when $\varepsilon < 1.2$, intermediate to clear for $\varepsilon \approx 2\sim3$, and then becomes clearer towards very clear conditions as $\varepsilon > 6.2$. This research focuses on clear sky condition. Therefore the sky clearness factor is controlled above 3 by adjusting the sunlight lumen ratio. Three lumen ratios were selected corresponding to three intervals. It can be seen that with the increase of sky clearness factor, the horizontal sunlight illuminance ratio rises from 0.55 to nearly 1. It is important to mention that the sunlight lumen ratio will be used to demonstrate simulation results for better comparison and illustration, but the sky clearness factor would be used in data regression for the purpose of practical application.

Table 1. Comparisons of sunlight lumen ratio, horizontal sunlight illuminance ratio and sky clearness factor and corresponding sky conditions

Sunlight lumen ratio (φ_{lumen})	Horizontal sunlight illuminance ratio	Sky clearness factor (ε)	Sky condition

1:9	0.55~0.75	3~3.6	Clear sky
1:4	0.75~0.85	3.6~6.6	Clear sky - Very clear sky
1:1	0.85~1	>6.6	Very clear sky

2.3 Multiple nonlinear regression

Multiple nonlinear regression is a kind of regression analysis by which the relationship between observation data can be described using a function. The dependent variable is determined by several independent variables through nonlinear combinations in a multiple nonlinear regression model. XLSTAT is a powerful and intuitive data analysing and statistical add-in integrated into Microsoft Excel, which provides user-friendly interface by Visual Basic Application (VBA) and mathematical and statistical computations by C++ (SARL, 2016). More than 100 statistical procedures for data analysis, regression, visualization and forecasting are offered by this program. In addition, it was claimed by the Addinsoft SARL that the results by XLSTAT are reliable due to the intensive tests against other software (SARL, 2016). In order to find the relations between several independent variables, the nonlinear regression using least-squares method would be applied to find the equation with the assumption of homoscedasticity which means the standard errors of regression is independent of the constant variance. The Levenberg-Marquardt and other complex but efficient algorithm would be used.

The criteria utilized to offer the goodness of regression are the coefficient of determination (R^2), the sum of squared errors (SSE) and the mean square error (MSE) as shown in Eq. 3-Eq. 6. There is no absolute criteria for a good value of R^2, MSE and SSE, and all of them should be considered when comparing the prediction data (Nau, n. d.). Generally speaking, the closer to 1 of R^2, the more accurate of prediction; the value of MSE smaller than 10% could be considered as the 'high' of accuracy preference (Lewis, 1982, Nau, n. d.).

$$R = \frac{n\sum y_i\hat{y}_i - (\sum y_i)(\sum \hat{y}_i)}{\sqrt{n(\sum y_i^2) - (\sum y_i)^2}\sqrt{n(\sum \hat{y}_i^2) - (\sum \hat{y}_i)^2}} \qquad (Eq. 3)$$

Where R is correlation coefficient; R^2 is coefficient of determination; $\hat{y}_i$ is the value of the dependent variable predicted by the model; y_i is the true value of the dependent variable; n is the number of samples.

$$SSE = \sum_{i=1}^{n} e_i^2 \qquad (Eq. 4)$$

$$e_i = y_i - \hat{y}_i \qquad (Eq. 5)$$

Where SSE is the sum of squared errors of prediction; e_i is the residual.

$$MSE(XLSTAT) = \frac{SSE}{DF} \qquad (Eq. 6)$$

Where DF is the degree of freedom.

2.4 Independent variables

In terms of independent variables, sun position is the most important factor that affects dCCPC performance, which can be described by both azimuth (γ) and altitude (θ_h). In order to find a more accurate and relatively complete result of how the sun influences the performance of dCCPC, the sky models with different sun locations were used in simulations in order to cover the likely incident angles as many as possible. Fig. 2 illustrates the schematic of dCCPC and sun positions used in simulations. The dCCPC was assumed to be positioned as the two perpendicular median planes are along the east-west and north-south directions. With the considerations of the symmetry of dCCPC and simplifying simulation, the solar azimuth was chosen from 0° to 45° with interval of 5°. When the sun is at very low altitude, the incident light entering dCCPC is quite few so that this condition does not need to be considered. Thus the solar altitude was chosen from 10° to 90° in every 5°. The combinations of the total 17 altitude angles and 10 azimuth angles give 170 sun locations in total which cover an eighth of the hemisphere of sky dome. For the incident ray whose azimuth or altitude is beyond its range, the azimuth or altitude angle can be converted to equivalent angle based on the symmetry of dCCPC for calculation. For example, for an incident ray having the azimuth of 243° and the altitude of 73°, the equivalent azimuth and altitude should be 27° and 73°.

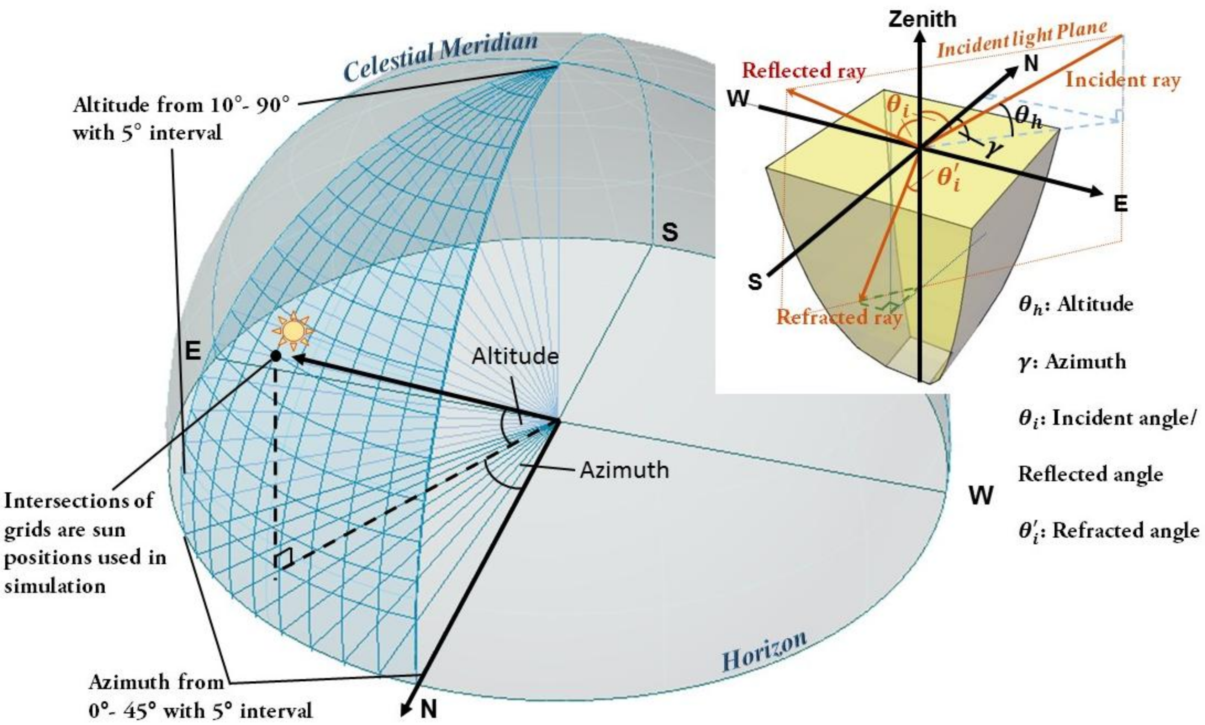

Figure 2. Schematic of azimuth, altitude and selected sun positions for simulation

The performance of dCCPC under overcast sky can be calculated by its geometric properties directly and it is almost constant for diffuse solar radiation (Rabl et al., 1980, Su et al., 2012b). The sky condition being focused on in this study is clear sky only. According to the realistic weather data (EnergyPlus, n.d.), the skylight and sunlight illuminance change all the time depending on the sun position and sky condition as well. In order to investigate the effects on CPC performance from sky conditions, sky clearness factor was applied as another independent variable. For each of the three ranges of sky clearness factor shown in Table 1, simulations were taken for total 170 sun positions as mentioned before. Therefore there were 510 sets of data in total were used to derive every mathematical model in this study.

2.5 Dependent variables

Transmittance and optical efficiency are two main properties to evaluate the performance of dCCPC, and they will be the dependent variables in regressions. Transmittance indicates the amount of incident light passed through dCCPC. Optical efficiency reveals how much irradiance is received by the base of dCCPC, and it is for base-coated dCCPC only. They are expressed by Eq. 7 and Eq. 8 as follows:

$$T = \frac{E}{E_0} \quad (Eq.7) \quad \text{and} \quad \eta_{opt} = \frac{I_{obs}}{I_0} \quad (Eq.8)$$

Where E is the transmitted daylight illuminance; E_0 and I_0 are the illuminance and irradiance incident onto the entry aperture of dCCPC; T is the transmittance of dCCPC; η_{opt} is the optical efficiency of dCCPC; I_{obs} is the irradiance received by dCCPC base.

3. Results and regression

In this section, the simulation results will be presented and data regression will be put forward. There are three regressors which are altitude (θ_h), azimuth (γ) and sky clearness factor (ε), and two dependent variables that are transmittance (T) and optical efficiency (η_{opt}). Fig. 3 shows the flow chart of the regression models that will be introduced in this section. There are three regression models in total and each of them has three independent variables and one dependent variable. For each model, 510 groups of simulation data obtained from Photopia are provided. The investigation of regression model begins from non-coated dCCPC. Then the model will be adapted to base-coated dCCPC to see whether it is capable to predict its transmittance and optical efficiency.

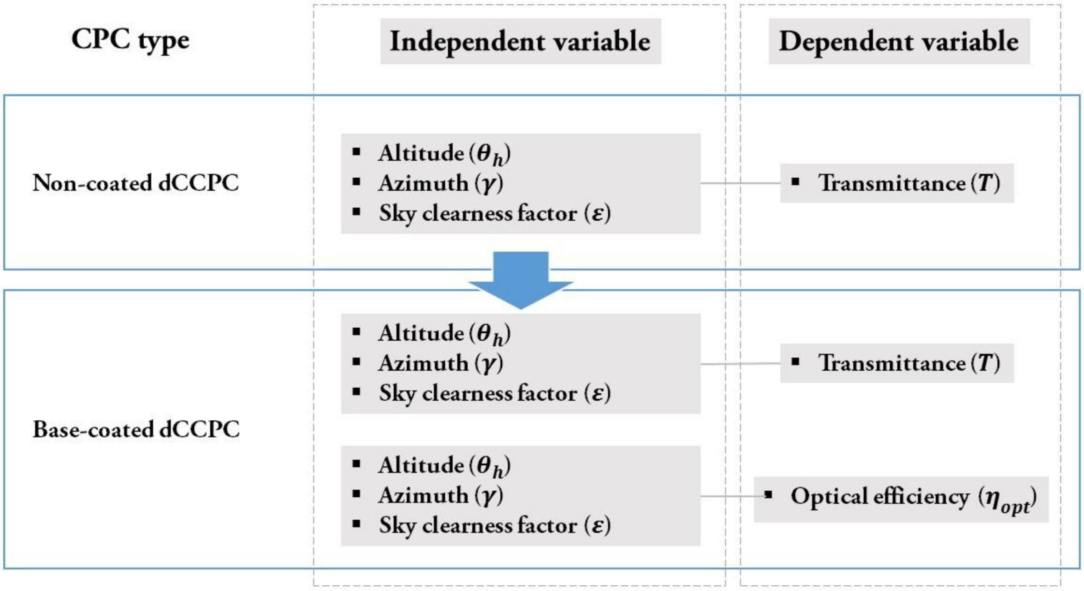

Figure 3. Independent and dependent variables used in data regression and prediction

3.1 Transmittance prediction model for Non-coated dCCPC

3.1.1 Simulation results

In accordance with different variables, massive simulation results were obtained by Photopia. Fig. 4 presents 3D contour plots of the transmittance of non-coated dCCPC varying with solar azimuth and altitude for sunlight lumen ratio of 1:9, 1:4, and 1:1 respectively; the transmittance under only direct sunlight condition is also presented in Fig. 4 a) as an ideal condition for comparison. It is verified that the transmittance does relate to these three criteria. When the incident light is direct sunlight only, the curved surface is the smoothest which is the best data set to investigate the relations between transmittance and sun position. When the dCCPC is under the both sun and sky dome, the transmittance becomes more and more uneven as the sunlight illuminance takes less and less percentage of total illuminance. Small peaks and valleys begin to occur on the curved surfaces of transmittance variation when the sunlight lumen ratio are 1:4 and 1:9. This is caused by the diffuse light emitted by sky dome in various directions.

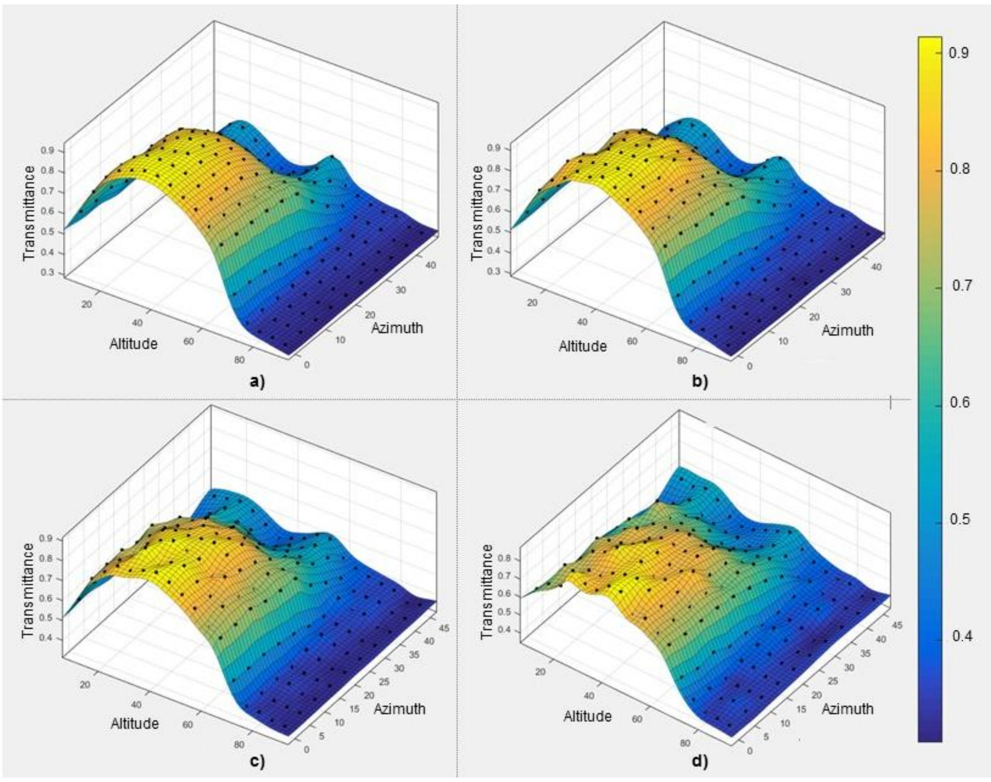

Figure 4. 3D contour plots of transmittance versus solar altitude and azimuth under clear sky with different sunlight lumen ratios in sky model (φ_{lumen}): a) only direct sunlight; b) $\varphi_{lumen} = 1:1$ $(\varepsilon \geq 6.6)$; c) $\varphi_{lumen} = 1:4$ $(\varepsilon \approx 3.6\text{~}6.6)$; d) $\varphi_{lumen} = 1:9$ $(\varepsilon \approx 3\text{~}3.6)$

Fig. 5 demonstrates how the sunlight lumen ratio in sky model affects transmittance and how transmittance varies with the two criteria more intuitively. The horizontal axis is divided into ten parts, and each part refers to a certain azimuth angle. In every part of azimuth, the curves show the transmittance changing with the altitude from 10° to 90°. The colours of curves distinguish different sunlight lumen ratios. It can be found that the peak values of transmittance decrease generally when the azimuth changes from 0° to 45°. When the azimuth ranges between 0°-30°, for a certain azimuth angle, the transmittance increases as the altitude rises from 10° to 35° and reaches the maximum value; then it drops with the altitude increasing from 35° to 90°; the transmittance is at the lowest value when the altitude is 90°. This performance presents how dielectric CCPC controls transmission of incident light. CCPC can receive incident light with an incident angle smaller than its half acceptance angle. Part of the light refracted into CCPC is escaped from the curved surfaces and edges causing transmittance; the rest of light is reflected out of CCPC again after total internal reflection. When the incident light is located at higher altitude angle (45°-90), more incident light will be reflected out so that the transmittance decreases. When the azimuth angle of incident light is within 35°-45°, the transmittance declines slightly on the original tendency as the altitude is at 20°-55°. Because CCPC consists of only four parabolic surfaces, there is no parabolic surface facing the direction from which the azimuth of incident light is close to 45°. More complicated total internal reflections occur inside CCPC which may cause the fluctuation of transmittance variation. In addition, it can be observed that the effects by sunlight lumen ratio in sky model are not significantly. It mainly changes the peak and lowest values of transmittance but does not influence the tendencies of transmittance variation. Comparing with the two curves of only direct sunlight and sunlight lumen ratio of 1:9 in sky model, the maximum difference of transmittance is ± 0.1 approximately. It is important to mention that the altitude and azimuth are the critical criteria affecting transmittance of non-coated CCPC; the sky clearness factor does not has significant influence on it: It changes the peak and valley values regardless of the variation tendency.

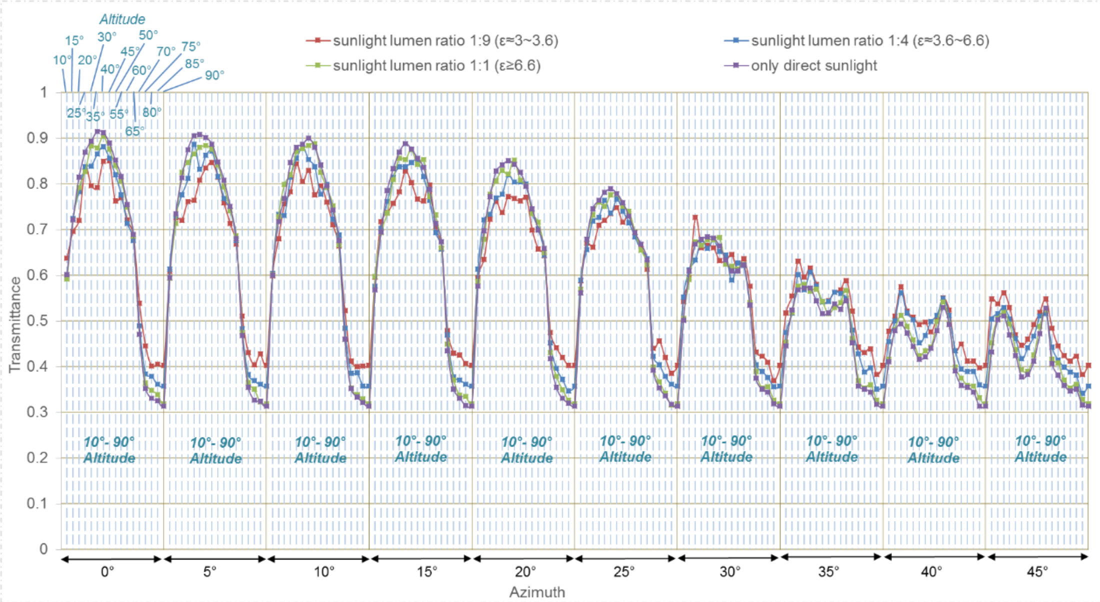

Figure 5. Transmittance of non-coated CCPC under clear sky with different sunlight lumen ratios in sky model (Altitude of sun ranges from 10°-90°; Azimuth of sun ranges from 0°-45°)

3.1.2 Regression prediction model

Based on the simulation results, twelve regression equations that are likely to provide strong correlations are proposed as shown in Table 2 below. The goodness of each regression equation is demonstrated in Table 3. In every regression, the independent variables are altitude (θ_h), azimuth (γ) and sky clearness factor (ε); the dependent variable is transmittance (T). The regression starts from the most common way, the first order polynomial equation, as expressed by Eq. 9-1. It is obvious that this equation does not fit well according to the low R^2 of 0.572 in this regression. It was found that the variations of transmittance are periodic with the change of azimuth and altitude. Thus the terms including altitude (θ_h) and azimuth (γ) in polynomial equation are replaced by trigonometric functions in Eq. 9-2, 9-3 and 9-4. The goodness of these equations indicates the trigonometric functions make the regressions fit simulation data better. For Eq. 9-4, the coefficient of determination R^2 reaches 0.836. However the sum of squared errors (SSE) of predictions for this equation is not good enough. Then the quadratic polynomial functions as shown by Eq. 9-5 and 9-6 are attempted but the fittings are almost the same as the first order polynomial equation. In regression equation, the main effect and interaction effect should be taken into account (Michigan, n.d.). Up to now each independent variable has been incorporated into the regression equation as a main-effect term however the regressions are not satisfied. The interactions among these variables are considered beginning with Eq. 9-7. In Eq. 9-7 and 9-8, the functions with the multiplication of independent variables are tried but they still do not provide satisfactory regression results. However, when plotting the regression results of Eq. 9-8 it was found that this equation provides comparable tendencies of transmittance variation compared to simulation results although it does not perform acceptable goodness of regression. Then, Eq. 9-9 is proposed which contains the interactions between only two independent variables: azimuth and altitude. This equation provides relatively good fittings with the high R^2 of 0.915. It also inspired the authors to fit data in a new way. Because the variations of transmittance are mainly determined by azimuth and altitude, and the sky clearness factor does not affect the variation of tendencies. In regression equation, the multiplication of two terms with trigonometric functions of altitude and azimuth are applied to determine the general variations of predicted values; then another term with sky clearness factor is multiplied by them as correction. Therefore Eq. 9-10, 9-11 and 9-12 are put forward. The third term of interaction is polynomial function. It was found that the regressions coincide with simulated data well when the correction term contains all of the three independent variables. Comparing with the fitting goodness of these three equations, it can be seen that when the order of polynomial function in correction term is higher, the regression fits the simulated data better. When the order of polynomial function is higher than 3, the goodness stays stable. Based on the goodness and simplification of regression, Eq. 9-12 is decided to be the regression equation to forecast the transmittance of non-coated dCCPC. Because there is no skylight in the models simulating the data set of 'only direct sunlight', it is important to mention that this data set was not used for the regression in Eq. 9-12.

Table 2. Regressing equations attempted for the correlations of altitude, azimuth and sky clearness factor to the transmittance of non-coated dCCPC

Eq. 9-1	$T = a_1\theta_h + a_2\gamma + a_3\varepsilon + a_4$
Eq. 9-2	$T = a_1 \cos\theta_h + a_2 \cos\gamma + a_3\varepsilon + a_4$
Eq. 9-3	$T = a_1 \cos(b_1\theta_h) + a_2 \cos(b_2\gamma) + a_3\varepsilon + a_4$
Eq. 9-4	$T = a_1 \cos(b_1\theta_h + b_2) + a_2 \cos(b_3\gamma + b_4) + a_3\varepsilon + a_4$
Eq. 9-5	$T = a_1\theta_h^2 + a_2\gamma^2 + a_3\varepsilon^2 + a_4$
Eq. 9-6	$T = a_1 \cos^2(b_1\theta_h + b_2) + a_2 \cos^2(b_3\gamma + b_4) + a_3\varepsilon^2 + a_4$
Eq. 9-7	$T = a_1\theta_h \cdot \gamma \cdot \varepsilon + a_2$
Eq. 9-8	$T = a_1 \cos(b_1\theta_h + b_2) \cdot \cos(b_3\gamma + b_4) \cdot \varepsilon + a_2$
Eq. 9-9	$T = a_1 \cos(b_1\theta_h + b_2) \cdot \cos(b_3\gamma + b_4) + a_2$
Eq. 9-10	$T = a_1 \cos(b_1\theta_h + b_2) \cdot \cos(b_3\gamma + b_4) \cdot (c_1 + c_2\varepsilon + c_3\gamma + c_4\theta_h + c_5\theta_h\gamma + c_6\varepsilon\gamma + c_7\theta_h\varepsilon + c_8\varepsilon\theta_h\gamma) + a_2$
Eq. 9-11	$T = a_1 \cos(b_1\theta_h + b_2) \cdot \cos(b_3\gamma + b_4) \cdot \left(c_1 + c_2\varepsilon + c_3\gamma + c_4\theta_h + c_5\theta_h\gamma + c_6\varepsilon\gamma + c_7\theta_h\varepsilon + c_8\varepsilon^2\theta_h\gamma + c_9\theta_h^2\varepsilon\gamma + c_{10}\gamma^2\varepsilon\theta_h + c_{11}\varepsilon^2\theta_h^2\gamma^2\right) + a_2$
Eq. 9-12	$T = a_1 \cos(b_1\theta_h + b_2) \cdot \cos(b_3\gamma + b_4) \cdot \left(c_1 + c_2\varepsilon + c_3\gamma + c_4\theta_h + c_5\theta_h\gamma + c_6\varepsilon\gamma + c_7\theta_h\varepsilon + c_8\varepsilon^2\theta_h\gamma + c_9\theta_h^2\varepsilon\gamma + c_{10}\gamma^2\varepsilon\theta_h + c_{11}\varepsilon^2\theta_h^2\gamma^2 + c_{12}\varepsilon^2 + c_{13}\theta_h^2 + c_{14}\gamma^2\right) + a_2$

θ_h is altitude (expressed in radian measure); γ is azimuth (expressed in radian measure); ε sky clearness factor; T is transmittance; a_n, b_n, c_n are regression coefficients.

Table 3. Goodness of regressions (Eq. 9-1 – Eq. 9-12) for non-coated dCCPC

Eq. No.	R^2	SSE	MSE	RMSE	Eq. No.	R^2	SSE	MSE	RMSE
Eq. 9-1	0.572	6.346	0.013	0.112	**Eq. 9-7**	0.174	12.241	0.024	0.155
Eq. 9-2	0.676	4.799	0.009	0.097	**Eq. 9-8**	0.476	7.771	0.015	0.124
Eq. 9-3	0.695	4.517	0.009	0.095	**Eq. 9-9**	0.915	1.840	0.003	0.052
Eq. 9-4	0.836	2.434	0.005	0.070	**Eq. 9-10**	0.933	0.995	0.002	0.045
Eq. 9-5	0.696	4.502	0.009	0.094	**Eq. 9-11**	0.937	0.938	0.002	0.044
Eq. 9-6	0.838	2.405	0.005	0.069	**Eq. 9-12**	0.944	0.825	0.002	0.041

R^2: coefficient of determination; SSE: sum of squared errors of prediction
MSE: mean squared error; RMSE: root mean square error

For the simulated non-coated dCCPC, Table 4 illustrates the parameter values obtained for regression Eq. 9-12. The parameter values for Eq. 9-1 to Eq. 9-13 are presented in Table A. 1 in Appendix for the purpose of reproducing the outcomes in this paper. The coefficient of determination (R^2) of this regression model is 0.944 which indicates the regression is relative accurate and acceptable. In addition, it is important to mention that the altitude and azimuth angle used in this equation should be in radian measure. This equation is suitable when the altitude ranges between 10°-90° and the azimuth ranges from 0° to 45°. If the dCCPC is tilt or the incident light coming from other angles beyond the acceptable ranges of angles, this equation is still applicable by converting the angle of incident light to equivalent angles within the acceptable ranges on the basis of the symmetry of dCCPC. In addition, this equation should also be suitable for other designs of non-coated dCCPC but the parameter values would be different.

Table 4. Parameter values of Eq. 9-12 for predicting the transmittance of non-coated dCCPC

a_1	1.496188	c_2	0.002828	c_9	0.000495
a_2	0.406272	c_3	0.280238	c_{10}	-0.036059
b_1	2.036185	c_4	0.536357	c_{11}	0.000658
b_2	1.932737	c_5	-0.010543	c_{12}	-0.000065
b_3	1.564716	c_6	0.001939	c_{13}	-0.350158
b_4	3.308904	c_7	0.000824	c_{14}	-0.326153
c_1	0.100193	c_8	0.000047		

The simulation results and the values predicted by Eq. 9-12 with determined parameter values for transmittance of non-coated dCCPC are compared in Fig. 6. It can be seen that the regression data fits simulated data perfectly in no matter what interval of azimuth and transmittance. All of the predicted values are located within the region of $\pm$20% deviation, which implies that this mathematical model is reliable to predict the transmittance of non-coated dCCPC. It can be also seen that different from the incident light at 0°-30° azimuth angle, the transmittance of non-coated dCCPC is always lower than 0.6 when the light is incident at the azimuth angle within 30°-45°. The transmittance of non-coated dCCPC is larger than 0.3 for all incident angle of light.

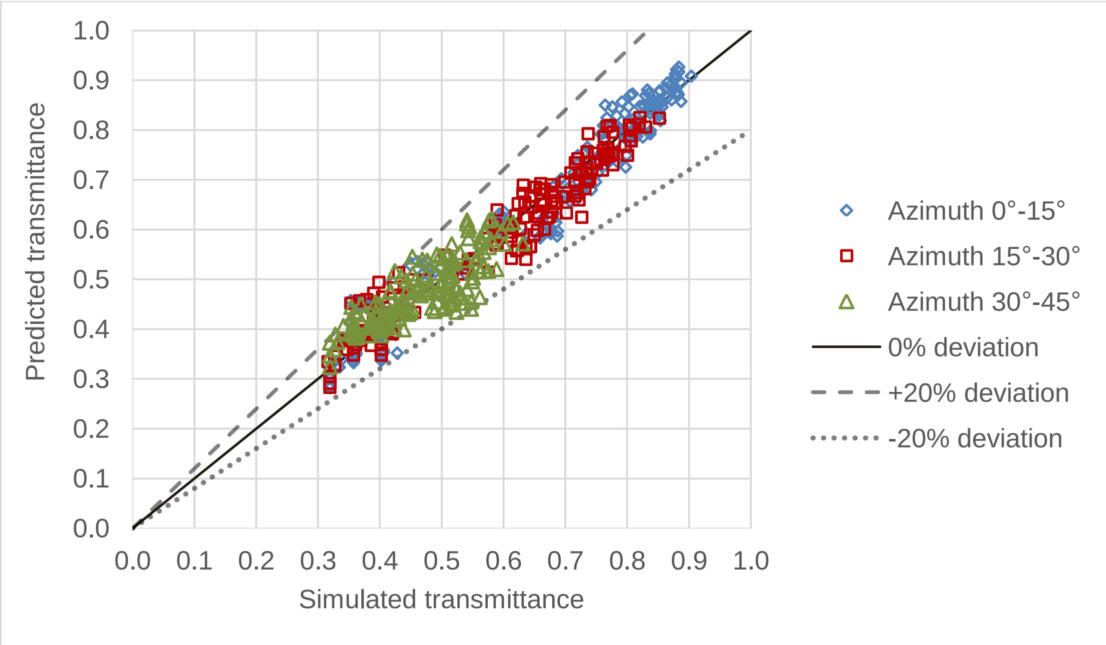

Figure 6. Comparisons between predicted and simulated transmittance of non-coated dCCPC (Regression: Eq. 9-12)

The absolute values of the residuals between predicted and simulated transmittance are quantified in Fig. 7. It can be found that all of the values are smaller than 0.12 and more than 80% of them are smaller than 0.06. For different azimuth and altitude angles, the residuals distribute relatively uniformly. When the altitude ranges from 10° to 50°, most of the residuals are smaller than 0.06. Larger residuals also occur when the altitude is between 55° and 75° for different azimuth angles.

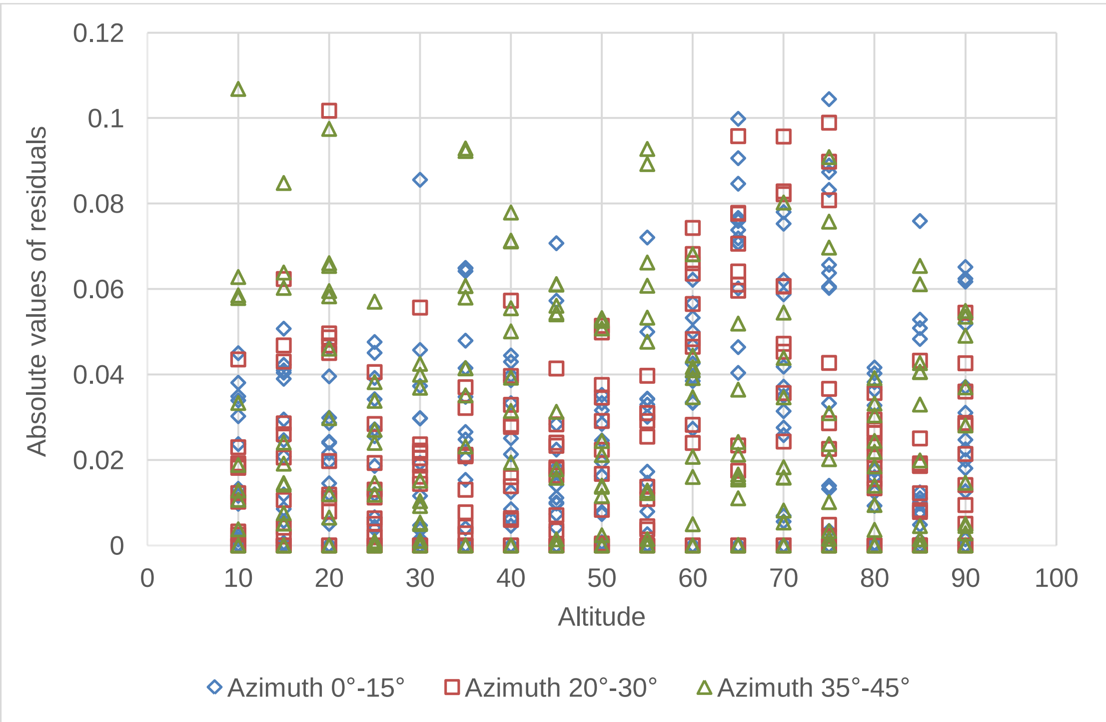

Figure 7. Absolute values of the residuals of predicted and simulated transmittance for non-coated dCCPC (Regression: Eq. 9-12)

3.2 Transmittance prediction model for base-coated dCCPC

Base-coated dCCPC has totally the same structure as non-coated dCCPC but possessing an absorbing surface attached on its base (exit aperture). The relationships obtained from ray-tracing simulation among transmittance, azimuth, altitude and sunlight lumen ratio in sky model of base-coated dCCPC are illustrated in Fig. 8. It can be seen that the tendencies of curves are almost same as those of non-coated dCCPC, but base-coated dCCPC performs similar maximum values and lower minimum values of transmittance. The maximum difference between transmittance for the two curves of only direct sunlight and sunlight lumen ratio of 1:9 in sky model is ± 0.2 approximately.

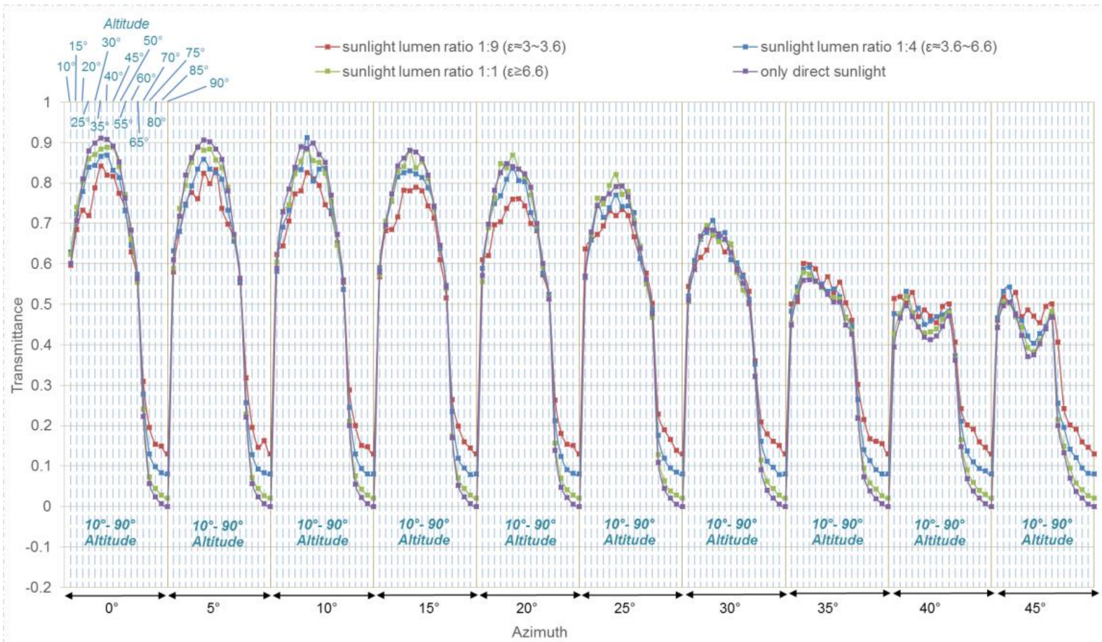

Figure 8. Transmittance of base-coated dCCPC under clear sky with different sunlight lumen ratios in sky model (Altitude of sun ranges from 10°-90°; Azimuth of sun ranges from 0°-45°)

Considering the similarities of the tendency and the periodicity between the transmittance for base-coated and non-coated dCCPC, it is supposed that the regression model for non-coated dCCPC is likely to predict the transmittance of base-coated dCCPC as well. Thus the simulation results for base-coated dCCPC were regressed using Eq. 9-12 and the correlations between simulation and prediction results are presented in Fig. 9. It can be seen that most of the predicted values are located within the region of ±20% deviation. The goodness of this regression model provides the 0.967 of R^2 and 1.234 of SSE, which indicates that the regression Eq. 9-12 is still suitable to predict the transmittance for base-coated dCCPC, but big deviations appear when the transmittance is smaller than 0.3 regardless of azimuth angle.

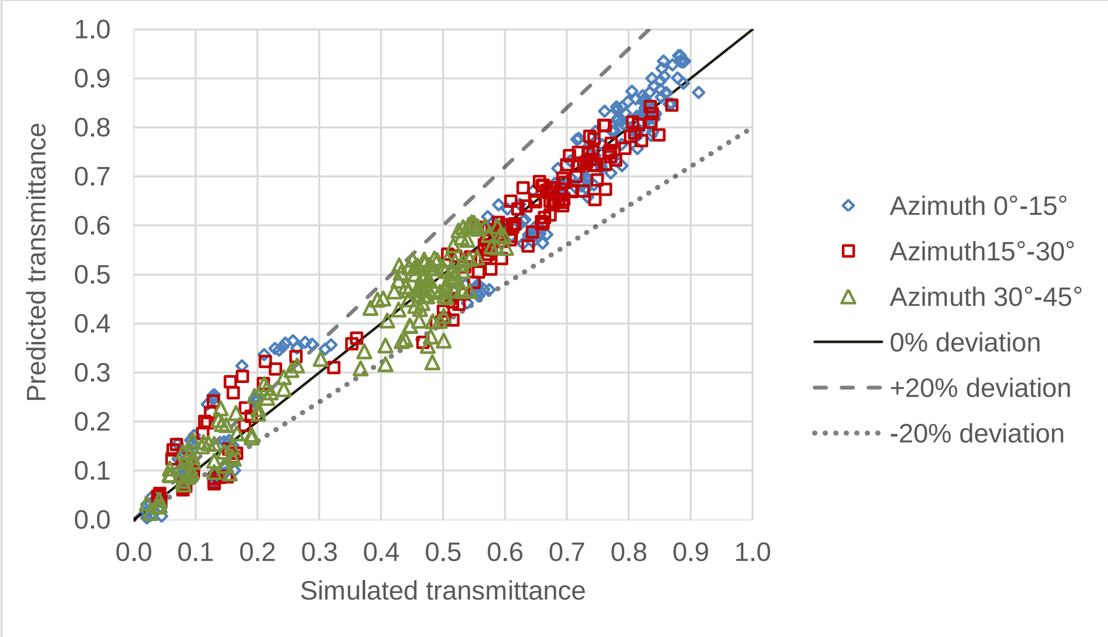

Figure 9. Comparisons between predicted and simulated transmittance of base-coated dCCPC (Regression: Eq. 9-12)

According to the transmittance results shown in Fig. 8, it can be seen that for each different azimuth angle, the transmittance of base-coated dCCPC is lower than 0.3 when the altitude of incident light ranges from 70° to 90°. The reason of larger errors occurring at lower transmittance may be because the regression parameters are not perfectly suitable for the whole range of the data. Thus, it is attempted to divide all of the transmittance results into two groups: one is that the altitude is smaller than 70° the other is that the altitude is equal to or larger than 70°; then two groups of parameter values are regressed according to Eq. 9-12. The value of each parameter is obtained as shown in Table 5 and the comparisons between predicted and simulated values are illustrated in Fig. 10. It can be found that with the new parameter values, almost all of the deviations for predicted transmittance are within the range of -20% - 20% compared to the original simulation results. A few large errors occur when the transmittance is within 0.4-0.5 and the azimuth angle ranges between 30° and 45°. This is caused by the transmittance having the slightly different tendencies compared to the transmittance of other azimuth angles, which can be found in Fig. 8. For all of the data in two groups, the goodness of prediction is 0.986 of R^2 and 0.531 of SSE, which is better than the regression by using only one group of parameter values. It is suggested that using two groups of parameter values for more accurate transmittance prediction of base-coated dCCPC.

Table 5. Parameter values of Eq. 9-12 for predicting the transmittance of base-coated dCCPC

Parameter values of Eq. 9-12 (θ_h≥70°)					
a_1	15.438580	c_2	0.000189	c_9	0.000041
a_2	0.272134	c_3	0.028146	c_{10}	0.001606
b_1	3.172319	c_4	0.156169	c_{11}	-0.000020
b_2	1.971506	c_5	-0.020172	c_{12}	-0.000003
b_3	1.376607	c_6	-0.000187	c_{13}	-0.042172
b_4	3.076578	c_7	0.000103	c_{14}	0.005846

c_1	-0.128884	c_8	-0.000001		
Parameter values of Eq. 9-12 (θ_h<70°)					
a_1	1.103238	c_2	0.015591	c_9	-0.039893
a_2	-0.437428	c_3	-2.844649	c_{10}	-0.008916
b_1	1.567036	c_4	-0.589013	c_{11}	0.000383
b_2	2.297709	c_5	-0.825488	c_{12}	-0.000403
b_3	0.584756	c_6	-0.015636	c_{13}	1.138829
b_4	1.968326	c_7	0.005027	c_{14}	1.331796
c_1	2.870284	c_8	0.001094		

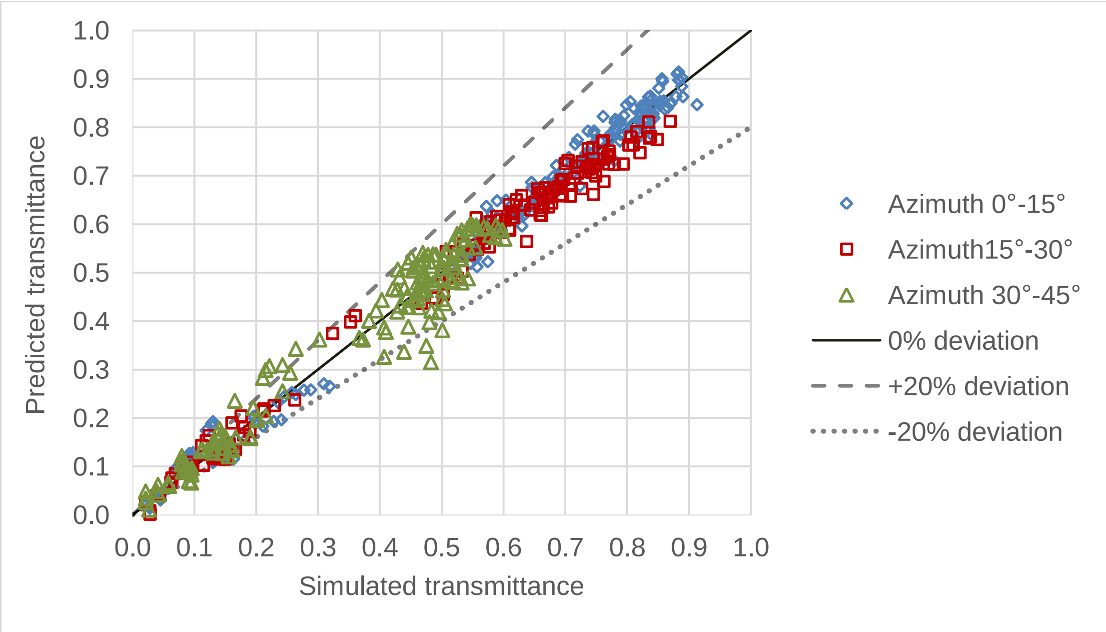

Figure 10. Comparisons between predicted and simulated transmittance of base-coated dCCPC (Regression: Eq. 9-12, separate parameter values for θ_h≥70° and θ_h<70°)

3.3 Optical efficiency prediction model for base-coated dCCPC

For base-coated dCCPC, another important characteristic is optical efficiency except for transmittance. In order to find whether the optical efficiency has similar relations with these criteria, they are plotted in Fig. 11 in the same way. It is interesting to see that the optical efficiency is mainly determined by solar altitude, in other words, the incident angle of light. The optical efficiency does not change as obviously as transmittance with variation of azimuth. When the solar altitude is at around 70°, there is a steep increase of optical efficiency which indicates that most of the light is concentrated onto the base of dCCPC when the light is incident within the half acceptance angle of dCCPC. The sunlight lumen ratio in sky model has similar influences on it compared to transmittance. The differences of the optical efficiencies under 1:9 sunlight lumen ratio and only direct sunlight range from -0.2 to +0.05 approximately.

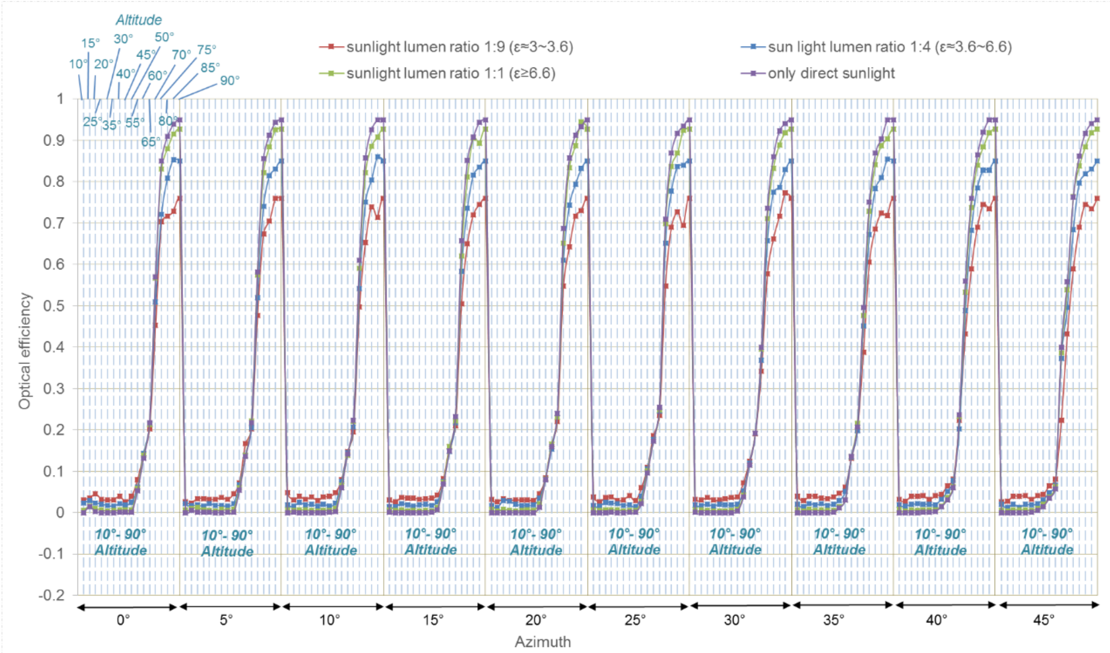

Figure 11. Optical efficiency of base-coated dCCPC under clear sky with different sunlight lumen ratio in sky model (Altitude of sun ranges from 10°-90°; Azimuth of sun ranges from 0°-45°)

In accordance with the relationships among optical efficiency, altitude, azimuth and sky clearness factor shown in Fig. 11, it was found that the optical efficiency of base-coated dCCPC has the same periodicity with transmittance: the optical efficiency varies in similar tendencies for different altitudes, and it changes with altitude for a certain azimuth. Thus, Eq. 9-12 is also attempted to predict the optical efficiency and the new expression formula is written as Eq. 9-13. The goodness of regression provides the R^2 of 0.969 and SSE of 1.760 which shows the regression is satisfactory in general. Fig. 12 illustrates the scatterplot comparing the predicted and simulated values for the regression. Similar to the regression for transmittance of base-coated dCCPC, the predicted optical efficiency has relatively larger deviation when the optical efficiency is smaller than 0.3. Thus, all of the results are attempted to be divided into two groups for separate regressions.

$$\eta_{opt} = a_1 \cos(b_1\theta_h + b_2) \cdot \cos(b_3\gamma + b_4) \cdot \left(c_1 + c_2\varepsilon + c_3\gamma + c_4\theta_h + c_5\theta_h\gamma + c_6\varepsilon\gamma + c_7\theta_h\varepsilon + c_8\varepsilon^2\theta_h\gamma + c_9\theta_h^2\varepsilon\gamma + c_{10}\gamma^2\varepsilon\theta_h + c_{11}\varepsilon^2\theta_h^2\gamma^2 + c_{12}\varepsilon^2 + c_{13}\theta_h^2 + c_{14}\gamma^2\right) + a_2 \qquad (Eq. 9-13)$$

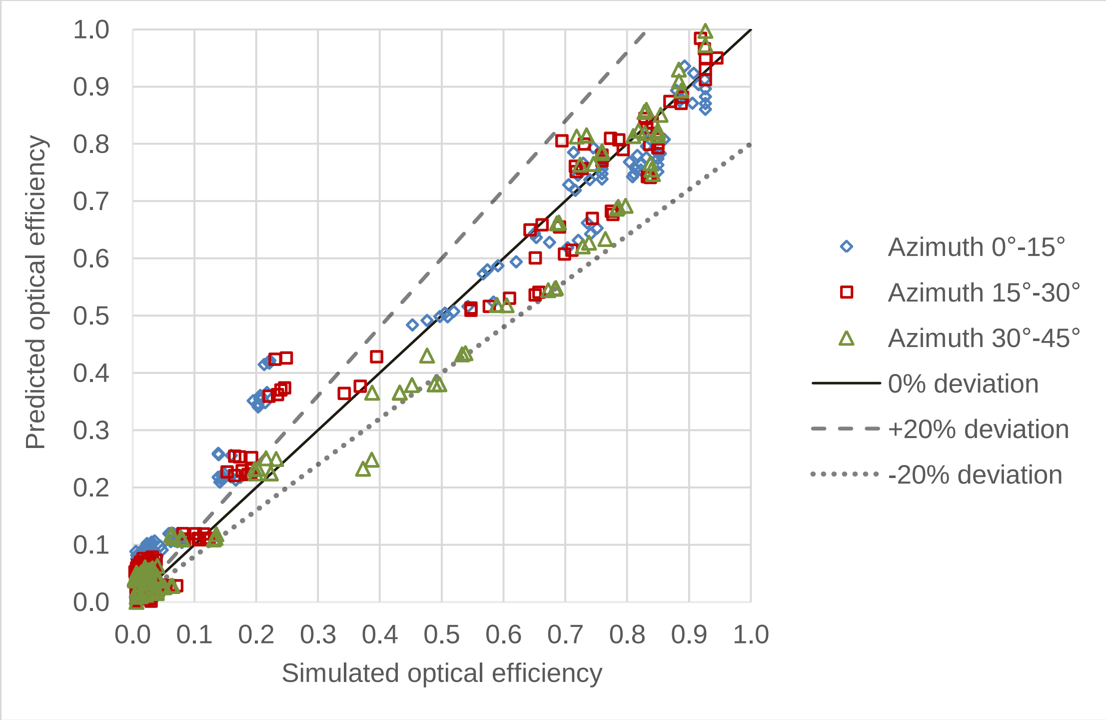

Figure 12. Comparisons between predicted and simulated optical efficiency of base-coated dCCPC (Regression: Eq. 9-13)

According to the variations of optical efficiency shown in Fig. 11, it was found that the 70° of altitude is the boundary determining whether the optical efficiency is less than or higher than 0.3 for most of the data. The regressions are conducted for the data that with the altitude equal to or larger than 70°, and less than 70°. The parameter values of regressions are listed in Table 6 and the comparisons between predicted and simulated results are illustrated in Fig. 13. For the new regression results, the R^2 is 0.994 and the SSE is 0.349, which implies the regression fits better when separating the data into two groups for regressions. Almost all of the predicted values are located within the range of ±20% deviation. The regression results indicate that the derived mathematical model can be applied for not only transmittance, but optical efficiency for dCCPC.

Table 6. Parameter values of Eq. 9-13 for predicting the optical efficiency of base-coated dCCPC

Parameter values of Eq. 9-12 (θ_h≥70°)					
a_1	5.232485	c_2	-0.002435	c_9	-0.000384
a_2	-0.355704	c_3	-0.311694	c_{10}	-0.000638
b_1	2.121739	c_4	0.415850	c_{11}	0.000010
b_2	2.812218	c_5	0.213677	c_{12}	0.000010
b_3	0.581986	c_6	-0.003565	c_{13}	-0.114970
b_4	3.322576	c_7	0.000789	c_{14}	-0.066297
c_1	-0.594695	c_8	0.000065		
Parameter values of Eq. 9-12 (θ_h<70°)					
a_1	0.365010	c_2	0.068264	c_9	-0.162943
a_2	0.046430	c_3	2.316287	c_{10}	0.135648
b_1	4.133090	c_4	4.273429	c_{11}	-0.008014

b_2	1.081834	c_5	-1.633847	c_{12}	-0.002401
b_3	0.382385	c_6	-0.151169	c_{13}	-3.873164
b_4	1.776869	c_7	-0.001518	c_{14}	-0.661668
c_1	-1.801165	c_8	0.012119		

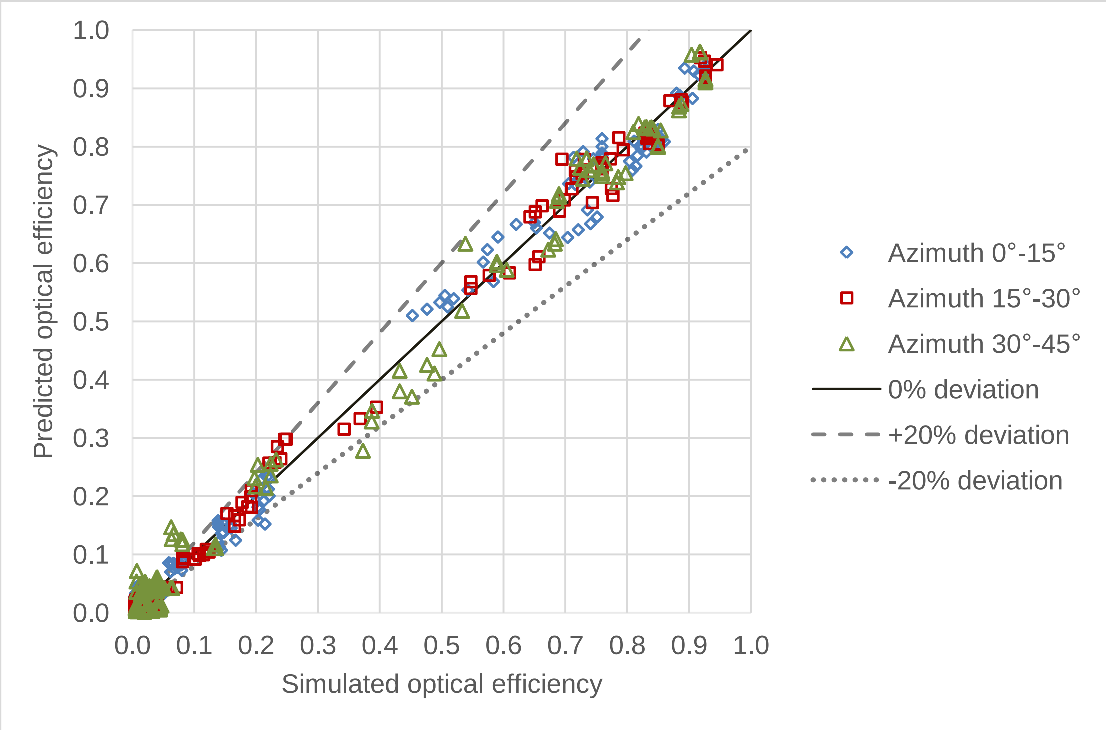

Figure 13. Comparisons between predicted and simulated optical efficiency of base-coated dCCPC (Regression: Eq. 9-12, separate parameter values for θ_h≥70° and θ_h<70°)

4. Discussion

4.1 Verification of prediction models

In this section, several examples of predicting the optical performance for the simulated dCCPC will be presented to show using derived regression models in practice, as well as to verify the feasibility of the prediction method. The location of Nottingham, UK (53.0°N, 1.2°W) will be used as an example. The time and date selected are the 10am and 12pm for spring equinox (21st Mar), summer solstice (21st Jun) and winter solstice (21st Dec). The dCCPC is assumed to be located facing south with the tilt angle 37°, which can collect the most sunlight. The comparisons between predicted and simulated values for the selected date and time are demonstrated in Table 7. For the three regression models, the predicted results are close to the simulated results. The deviations between them are mostly smaller than 0.1. The biggest error of 0.14 occurs in the transmittance prediction at 10am on 21st Dec. It can be seen that the prediction models are reliable to predict the optical performance for dCCPC in practical conditions.

Table 7. Verification of predicted optical performance to simulation results for dCCPC on various dates and times

Local time			21 Mar		21 Jun		21 Dec	
			10am	**12pm**	**10am**	**12pm**	**10am**	**12pm**
Solar altitude			29.9°	36.5°	52.0°	60.4°	9.1°	13.6°
Solar azimuth			141.0°	176.2°	128.7°	177.1°	151.8°	179.5°
Tilt angle (β)			37°	37°	37°	37°	37°	37°
sky clearness factor (*ε*)			4.42	3.04	5.58	6.56	5.29	8.48
Non-coated dCCPC	transmittance	predicted	0.68	0.47	0.67	0.37	0.57	0.81
		simulated	**0.73**	**0.44**	**0.71**	**0.37**	**0.50**	**0.84**
Base-coated dCCPC	transmittance	predicted	0.63	0.28	0.55	0.12	0.59	0.78
		simulated	**0.64**	**0.23**	**0.61**	**0.09**	**0.45**	**0.83**
	optical efficiency	predicted	0.08	0.61	0.24	0.79	0.08	0.04
		simulated	**0.09**	**0.74**	**0.22**	**0.83**	**0.02**	**0.02**

4.2 Model limitations

The regressions in this study are all based on the results simulated by Photopia which is an accurate raytracing tool. In order to introduce the feasibility of the obtained regression equation, it is important to describe the sky model used in simulations. The light distribution in sky model is calculated by IESNA RP-21 daylight equations (Photopia, n.d., IESNA, 1984). There are two kinds of sky models provided by Photopia lamp library, one is overcast sky and the other is clear sky. In the new sky standard published by the British Standard Institution, there are 15 luminance distributions for different sky conditions that are determined by the gradation (I-VI) and indicatrix (1-6) parameter numbers (B.S.I., 2004). The luminance distribution of the overcast sky model used in Photopia is the same as CIE Standard Overcast Sky model I.1 which has steep luminance gradation towards zenith, azimuthal uniformity. The clear sky model in Photopia is similar to the type V.4 (CIE Standard Clear Sky with low luminance turbidity) in CIE standard. For the clear sky model, part of sky that is near the sun would be brighter. The intensive light beams are emitted from the solar disk. Therefore, the sunlight would be the main factor that affects dCCPC performance in the simulations using clear sky model. Hence, the main limitation of the regression equations obtained is that they are suitable for the clear sky condition in which the sunlight illuminance is predominant.

4.3 Significance of prediction models

The results obtained from the best regression models for non-coated and base-coated dCCPCs are illustrated in Table 8 below. For the models forecasting the optical efficiency and transmittance, the high values of R^2 indicate their feasibility but few of predictions may have relatively large errors. The coefficient of determination (R^2) of all models are higher than 0.94 and the MSE are smaller than 0.002, which indicates they are capable to predict the nonlinear relationship reliably for the optical performance of both non-coated and base-coated dCCPCs.

Table 8. Summary of multiple nonlinear regression models

CPC type	Independent variables	Dependent variables	Regression		
			R^2	SSE	MSE
Non-coated	$\theta_h, \gamma, \varphi_{sun}$	T	0.944	0.825	0.0017
Base-coated	$\theta_h, \gamma, \varphi_{sun}$	T	0.986	0.531	0.0011
Base-coated	$\theta_h, \gamma, \varphi_{sun}$	η_{opt}	0.994	0.349	0.0007

The derived regression models provide a fast and simple approach to predict the optical performance of base-coated and non-coated dielectric dCCPC for the light coming from arbitrary directions accurately, which means the transmittance and optical efficiency of dCCPC can be determined directly under clear sky without running simulations by software when the tilt angle of dCCPC, sky clearness factor, time, longitude and latitude of location are given in practice. For example, for the solar concentrating photovoltaic (CPV) and solar thermal systems, they can be used to estimate the optical efficiency of dCCPC and then calculate the collected solar energy rapidly; in the daylighting control system integrated with dCCPC, the energy saving due to daylighting can be predicted accurately without the long-time simulations. On the other hand, the regression models proposed are suitable for not only the dCCPCs used in in this study, but also other CPCs with different dimensions owing to the similar structures and working principle of CPC. For other CPC of different geometries, the new parameter values of the proposed prediction equations can be obtained in the same way and then the specific model for it could be built.

6. Conclusion

The mathematical models for calculating the optical performance of dielectric crossed compound parabolic concentrator (dCCPC) have been proposed in this study through multiple nonlinear regression method in accordance to a mass of simulation results. The independent variables for each model are solar altitude, azimuth and sky clearness factor, which are used to determine both of the transmittance and optical efficiency of base-coated dCCPC and the transmittance of non-coated dCCPC. The coefficient of determination (R^2) for every model obtained by regression is higher than 0.94 and the deviations of most predicted data are less than 20% compared to simulation data, which indicates the accuracy and reliability of prediction models.

It is significant to establish the mathematical models for calculating the optical performance of dCCPC. The most common way to determine the optical performance of dCCPC is by raytracing simulation currently which requires a long time. The derived models can help to forecast the optical performance of dCCPC accurately and rapidly from the given solar altitude, solar azimuth and sky clearness factor, which saves a lot of time for running simulation. In addition, the regression models provide visualized equations that can be validated, optimized and it is friendly to be incorporated with other software. Meanwhile, it should be mentioned that the regression models proposed in this research are only suitable for the clear sky condition. The performance of dCCPC under overcast sky almost stays constant and can be calculated through its structural properties. This study only explored the prediction models for dCCPC, it is promising to adopt these models to predict the optical performance for other types of CPCs owing to the similar structure and working principles for the future work.

Acknowledgements

The authors would like to thank the European Commission for the Marie Curie Fellowship grant (H2020-MSCA-IF-2015-703746).

References

ARNAOUTAKIS, G. E., MARQUES-HUESO, J., IVATURI, A., FISCHER, S., GOLDSCHMIDT, J. C., KRMER, K. W. & RICHARDS, B. S. 2015. Enhanced energy conversion of up-conversion solar cells by the integration of compound parabolic concentrating optics. *Solar Energy Materials and Solar Cells,* 140**,** 217-223.

B.S.I., B. S. I. 2004. Spatial distribution of daylight - CIE standard general sky. BS ISO 15469:2004.

BAHAIDARAH, H. M., TANWEER, B., GANDHIDASAN, P., IBRAHIM, N. & REHMAN, S. 2014. Experimental and numerical study on non-concentrating and symmetric unglazed compound parabolic photovoltaic concentration systems. *Applied Energy,* 136**,** 527-536.

BAIG, H., SARMAH, N., CHEMISANA, D., ROSELL, J. & MALLICK, T. K. 2014a. Enhancing performance of a linear dielectric based concentrating photovoltaic system using a reflective film along the edge. *Energy,* 73**,** 177-191.

BAIG, H., SELLAMI, N., CHEMISANA, D., ROSELL, J. & MALLICK, T. K. 2014b. Performance analysis of a dielectric based 3D building integrated concentrating photovoltaic system. *Solar Energy,* 103**,** 525-540.

ENERGYPLUS 2016. EnergyPlus Version 8.7 Documentation - Engineering Reference. U.S. Department of Energy.

ENERGYPLUS. n.d. *EnergyPlus Weather Data* [Online]. National Renewable Energy Laboratory (NREL). Available: https://energyplus.net/weather [Accessed 5/21 2017].

IESNA, I. E. S. O. N. A. 1984. Calculation of Daylight Availability (IES RP-21). New York: IES.

KARATHANASSIS, I. K., PAPANICOLAOU, E., BELESSIOTIS, V. & BERGELES, G. C. 2017. Design and experimental evaluation of a parabolic-trough concentrating photovoltaic/thermal (CPVT) system with high-efficiency cooling. *Renewable Energy,* 101**,** 467-483.

KLEINDIENST, S., BODART, M. & ANDERSEN, M. 2008. Graphical Representation of Climate-Based Daylight Performance to Support Architectural Design. *LEUKOS: The Journal of the Illuminating Engineering Society of North America,* 5**,** 39-61.

LEWIS, C. D. 1982. *Industrial and business forecasting methods: a practical guide to exponential smoothing and curve fitting,* London, Butterworth scientific.

LI, G., PEI, G., JI, J. & SU, Y. 2015. Outdoor overall performance of a novel air-gap-lens-walled compound parabolic concentrator (ALCPC) incorporated with photovoltaic/thermal system. *Applied Energy,* 144**,** 214-223.

LI, G., PEI, G., SU, Y., JI, J. & RIFFAT, S. B. 2013. Experiment and simulation study on the flux distribution of lens-walled compound parabolic concentrator compared with mirror compound parabolic concentrator. *Energy,* 58**,** 398-403.

LI, G., PEI, G., SU, Y., WANG, Y. & JI, J. 2014a. Design and investigation of a novel lens-walled compound parabolic concentrator with air gap. *Applied Energy,* 125**,** 21-27.

LI, G., PEI, G., YANG, M., JI, J. & SU, Y. 2014b. Optical evaluation of a novel static incorporated compound parabolic concentrator with photovoltaic/thermal system and preliminary experiment. *Energy Conversion and Management,* 85**,** 204-211.

MALLICK, T. K. & EAMES, P. C. 2007. Design and fabrication of low concentrating second generation PRIDE concentrator. *Solar Energy Materials and Solar Cells,* 91**,** 597-608.

MALLICK, T. K., EAMES, P. C., HYDE, T. J. & NORTON, B. 2004. The design and experimental characterisation of an asymmetric compound parabolic photovoltaic concentrator for building façade integration in the UK. *Solar Energy,* 77**,** 319-327.

MALLICK, T. K., EAMES, P. C. & NORTON, B. 2006. Non-concentrating and asymmetric compound parabolic concentrating building façade integrated photovoltaics: An experimental comparison. *Solar Energy,* 80**,** 834-849.

MICHIGAN, U. O. n.d. *Multiple Linear Regression* [Online]. Available: http://dept.stat.lsa.umich.edu/~kshedden/Courses/Stat401/Notes/401-multreg.pdf [Accessed 5th April 2017].

NAU, R. n. d. *Statistical forecasting: notes on regression and time series analysis* [Online]. Available: https://people.duke.edu/~rnau/compare.htm [Accessed 19th Oct 2017].

PEREZ, R., INEICHEN, P., SEALS, R., MICHALSKY, J. & STEWART, R. 1990. Modeling daylight availability and irradiance components from direct and global irradiance. *Solar Energy,* 44**,** 271-289.

Photopia. n.d. *Photopia User's Guide.* [Online]. Available: http://www.ltioptics.com/en/photopia-standalone-base.html [Accessed 5th April 2017].

PIDERIT, M., CAUWERTS, C. & DIAZ, M. 2014. Definition of the CIE standard skies and application of high dynamic range imaging technique to characterize the spatial distribution of daylight in Chile. *Journal of Construction,* 13**,** 22-30.

RABL, A., O'GALLAGHER, J. & WINSTON, R. 1980. Design and test of non-evacuated solar collectors with compound parabolic concentrators. *Solar Energy,* 25**,** 335-351.

SARL, A. 2016. XLSTAT Help Documentation. Paris, FRANCE.

SARMAH, N. & MALLICK, T. K. 2015. Design, fabrication and outdoor performance analysis of a low concentrating photovoltaic system. *Solar Energy,* 112**,** 361-372.

SARMAH, N., RICHARDS, B. S. & MALLICK, T. K. 2014. Design, development and indoor performance analysis of a low concentrating dielectric photovoltaic module. *Solar Energy,* 103**,** 390-401.

SELLAMI, N. & MALLICK, T. K. 2013. Optical efficiency study of PV Crossed Compound Parabolic Concentrator. *Applied Energy,* 102**,** 868-876.

SELLAMI, N., MALLICK, T. K. & MCNEIL, D. A. 2012. Optical characterisation of 3-D static solar concentrator. *Energy Conversion and Management,* 64**,** 579-586.

SU, Y., PEI, G., RIFFAT, S. B. & HUANG, H. 2012a. Radiance/Pmap simulation of a novel lens-walled compound parabolic concentrator (lens-walled CPC). *Energy Procedia,* 14**,** 572-577.

SU, Y., RIFFAT, S. B. & PEI, G. 2012b. Comparative study on annual solar energy collection of a novel lens-walled compound parabolic concentrator (lens-walled CPC). *Sustainable Cities and Society,* 4**,** 35-40.

SUN, J. & SHI, M. Experimental Study on A Concentrating Solar Photovoltaic/Thermal System. Power and Energy Engineering Conference (APPEEC), 2010 Asia-Pacific, 28-31 March 2010 2010. 1-4.

TIAN, M. & SU, Y. 2015. A study on use of three-dimensional miniature dielectric compound parabolic concentrator (3D dCPC) for daylighting control application. *14th International Conference on Sustainable Energy Technologies -SET 2015.* Nottingham, UK.

TIAN, M. & SU, Y. 2016. three dimensional dielectric compound parabolic concentrator (3D dCPC) for daylighting control in roofing. *11th Conference on Advanced Building Skins.* Bern, Switzerland.

ULAVI, T., DAVIDSON, J. H. & HERBRINK, T. Analysis of a hybrid PV/T Concept based on wavelength selective films. ASME 2013 7th International Conference on Energy Sustainability, 2013 Minneapolis, Minnesota, USA, July 14–19, 2013.

ULAVI, T., HEBRINK, T. & DAVIDSON, J. H. 2014a. Analysis of a Hybrid Solar Window for Building Integration. *Energy Procedia,* 57**,** 1941-1950.

ULAVI, T., HEBRINK, T. & DAVIDSON, J. H. 2014b. Analysis of a hybrid solar window for building integration. *Solar Energy,* 105**,** 290-302.

WALZE, G., NITZ, P., ELL, J., GEORG, A., GOMBERT, A. & HOSSFELD, W. 2005. Combination of microstructures and optically functional coatings for solar control glazing. *Solar Energy Materials and Solar Cells,* 89**,** 233-248.

WELFORD, W. T. & WINSTON, R. 1978. *The optics of nonimaging concentrators - Light and solar energy*.

YU, X. & SU, Y. 2015. A discussion of inner south projection angle for performance analysis of dielectric compound parabolic concentrator. *Solar Energy,* 113**,** 101-113.

YU, X., SU, Y., ZHENG, H. & RIFFAT, S. 2014. A study on use of miniature dielectric compound parabolic concentrator (dCPC) for daylighting control application. *Building and Environment,* 74**,** 75-85.

ZACHAROPOULOS, A., EAMES, P. C., MCLARNON, D. & NORTON, B. 2000. Linear dielectric non-imaging concentrating covers for PV integrated building facades. *Solar Energy,* 68**,** 439-452.

Appendix

Table A.1. Parameter values of Eq. 9-1 - Eq. 9-11 for simulated non-coated dCCPC

Eq. 9-1	a_1	-0.232908	a_2	-0.315859	a_3	-0.000689	a_4	0.920885
Eq. 9-2	a_1	0.356634	a_2	0.843854	a_3	-0.000514	a_4	-0.372863
Eq. 9-3	a_1	5.013431	a_2	0.211949	a_3	-0.000492	a_4	-4.399681
	b_1	0.245632	b_2	2.183480				
Eq. 9-4	a_1	0.203053	a_2	0.830325	a_3	-0.000601	a_4	-0.204193
	b_1	3.043950	b_2	-1.946651	b_3	1.031683	b_4	-0.019142
Eq. 9-5	a_1	-0.148874	a_2	-0.401887	a_3	-0.000016	a_4	0.817815
Eq. 9-6	a_1	0.405930	a_2	0.546335	a_3	-0.000017	a_4	-0.127103
	b_1	1.515476	b_2	-0.970654	b_3	-1.006522	b_4	0.059443
Eq. 9-7	a_1	-0.008679	a_2	0.626795				
Eq. 9-8	a_1	0.014342	a_2	0.555678	b_1	-2.644212	b_2	1.610049
	b_3	2.469599	b_4	-0.235906				
Eq. 9-9	a_1	0.473580	a_2	0.397204	b_1	2.100950	b_2	-1.357810
	b_3	2.066359	b_4	-0.146640				
Eq. 9-10	a_1	-1.671734	a_2	0.385077	b_1	2.197839	b_2	1.568689
	b_3	0.261123	b_4	1.778506	c_1	-1.769722	c_2	-0.014123
	c_3	1.931195	c_4	0.587510	c_5	-0.536572	c_6	0.027779
	c_7	0.011019	c_8	-0.021769				
Eq. 9-11	a_1	-0.261408	a_2	0.408440	b_1	2.311628	b_2	1.511448
	b_3	1.923447	b_4	2.341663	c_1	-3.150923	c_2	-0.017137
	c_3	3.226629	c_4	1.155791	c_5	-1.119102	c_6	0.021083
	c_7	0.006956	c_8	0.000254	c_9	-0.012680	c_{10}	0.037775
	c_{11}	-0.000919						